SECTION 109

MULTISPECTRAL OBSERVATIONS OF MARINE ENVIRONMENTS

by

Fabian C. Polcyn
University of Michigan
Ann Arbor, Michigan

In previous reports (Ref. 1, 2) we have seen how the multispectral scanner has been used to map various features of the land and vegetation. In this paper we wish to demonstrate how the concept of the multispectral scanner, using multiple channels in registry and recorded on magnetic tape, can be used in variety of applications in the marine environment. In Fig. 1 we observe how the multiple bands spanning the ultraviolet through the visible and into the thermal infrared has been used, not only to detect the presence of the oil slick but also to permit its discrimination and possibly its thickness. Four test oil slicks were flown in cooperation with the U. S. Coast Guard (Ref. 3) and resulting tonal patterns can be observed. The different intensities across the four bands demonstrate clearly how the four oil types of different specific gravities can be discriminated.

A second application area is demonstrated in Fig. 2 where the results of mapping the benthic vegetation communities in the lower part of Biscayne Bay, Florida is shown. Originally the figure was in color and each color was used to isolate the particular vegetation community or bottom type i.e., sand or clay. The black represents the shoreline near Turkey Point. This work was done in cooperation with the U. S. Geological Survey (Ref. 4). These benthic communities were submerged under water at some 6 to 8 feet deep.

In the area of pollution monitoring, Fig. 3 is an example in three bands of a pollutant from a steel processing plant, and in this case we note that there is no contrast of the pollutant in the .55-.58 micrometer band, whereas the pollutant has a darker tone than the receiving waters in the .40-.44 μm, and it has a lighter tone than the receiving waters in the red band at .62-.66 μm. This variation of tone with wavelength can be emphasized by displaying the results on a graph of apparent reflectance vs. wavelength is shown in Fig. 4. In this case we see the result of a number of different effluents from different industries along the Detroit River, and we note how each has its own characteristic reflectance curve , thus suggesting the possibility of identification of a pollutant from its reflectance signature.

In a fifth area of application we have found that different light penetration capabilities into water at different wavelengths can be used to measure water depth. We constructed a model that will use ratios of spectral channels and with the proper auxillary information produce a depth

chart as illustrated in Fig. 5 (Ref. 5). The accuracies for such an example is shown in Fig. 6 where we compare the computed depth made with data from a multispectral scanner with depth soundings made for the same region. One can note that for depths down to 20 feet there is good agreement and as the depth increases resulting in smaller signal to noise ratios the uncertainties in the depth measurement becomes greater. This chart is for the test site 167 in the Lake Michigan beach areas in contrast to the previous example taken in the Florida Keys area.

The model that relates multispectral information to water depth has been developed using the geometry shown in the next figure (Fig. 7) where sunlight is the source of energy and the reflected radiation from the bottom is detected by the sensor. Ultimately the scanner should be operated with a laser ranging device on board the same aircraft that would supply an independent measure of sample depths thus allowing for the calculation of extinction coefficients of light in water and the ratio of bottom reflectances, removing the need for using average values.

When there is scattering of light in the water a modification is necessary before depths are calculated. In the next figure (Fig. 8) are the equations that were developed for relating the apparent reflectance developed from the scanner in terms of a bottom reflection modified by the effects of scattering, s, and absorption, α. Angles θ and ϕ are merely the angles of observation and incidence as shown in Fig. 7.

We have found that for best results in depth calculations between inshore and offshore waters in the Lake Michigan area, the scattering term must be taken into account. For a test area in this region, Fig. 9, we have calculated the relative attenuation coefficient for two areas, 80 feet from shore and 200 feet from shore where the depth goes down to 7-1/2 feet. There are differences in the attenuation coefficient due to the effects of suspended sediments and the increased scattering of light. Once this correction is made the accuracies in depth measurements for both inshore waters and offshore waters becomes greatly increased. This ability of the model to handle a scattering term is expected to be useful when we wish to begin calculations of the total quantities of pollutant or suspended sediments in a given outfall. Figure 10 is an illustration of why we think the spectra carries this quantity of information. The spectra taken directly at the outfall of one of the industrial discharges is compared to the sample taken 100 feet downstream and that in turn is compared to the spectrum from the Detroit River itself. The spectral shape demonstrates the dillution of the pollutant mixing with the river water. With a new model being developed we expect to take into account this dillution through the spectrum information and with the proper control points sampled from a boat, estimates on mass in suspension should be possible. As a minimum, calculation of concentration gradients should be possible even without having the control points, but for maximum utility some ground truth is needed.

Further application areas are illustrated by using high altitude photography supplied by NASA and taken on Mission 103. They also illustrate what may be possible with a satellite multispectral system in mapping the extent of shore currents, and beach erosion, and lake pollution on a wide area basis. Figure 11 is a black and white reproduction of a color photograph that shows evidence of complicated patterns of suspension in Lake Michigan near Frankfort, Michigan. The right hand portion of Crystal Lake, shown in the middle of the picture, shows a turbidity pattern which appears to be related to water quality degradation reported in this end of the lake by residents. In the top part of the picture we see the formation of a beach area through deposition of sand and formed by the coastal currents in this area. The higher altitude photography suggests that we can begin to understand the complicated circulation patterns involved in these coastal formations.

In another area of application, Fig. 12, we again see a photo taken at 60,000 feet by the NASA RB-57 of the ports of Muskegon and Grand Haven, Michigan. There is the outfall of a paper plant in Muskegon Lake and the distinct outline of the Grand River and Muskegon River discharges into Lake Michigan can be seen. Here shore currents are preventing these pollution laden waters from mixing completely with the deeper lake waters and in some cases the shore currents force the plumes inward along the beaches.

These shore currents are set up by prevailing winds and we believe they play a major role in the movement and deposition of sand along the Lake Michigan shores. In Fig. 13, we see this shore current, covering an area of one to two miles, by the sharp demarcation line representing different currents and the increase in turbidity associated with the transport of sand. Land protrusions into the lake upset these shore currents producing the eddy patterns shown in the figure. We can emphasize this offshore current formation again by referring to Fig. 14. Here the sharp boundaries between the current inshore and the lake can be seen by the discontinuity in the sun glitter pattern. Two different wave directions must be involved across the discontinuity. The dimensions of these shore currents should now be measureable with the use of such remotely sensed data.

In some cases these currents will trap the pollutant outfall from the rivers inshore. In Fig. 15 a river plume outline is actually trapped and brought into shore by the formation of this offshore current through wind processes. This is a phenomena that can happen any time during the spring, fall and summer, in contrast to the "thermal bar" effect which is essentially a spring phenomena. This particular thermal feature can be mapped using thermal infrared data. In Fig. 16 are the results of a flight line 14-1/2 miles in length along the Michigan shore between Muskegon and Port Sheldon. Depending on the wind condition, the thermal water masses from the Grand River, as well as from a power generating plant can be seen relative to the warm water created along the shore in spring due to the higher temperature of the land. In the April 22nd data, the "thermal bar" has not been formed

and most of the lighter tone (warmer temperature) areas are due to the outfalls of the Grand River. By the 30th of April we see a distinct boundary along the entire 14 mile strip, which by May 7 has moved farther offshore completing the annual cycle. The natural warming of these waters and the mixing of temperature zones can be seen in Fig. 17. Here for the 30th of April different temperatures slices are displayed for each temperature range. Through such analysis an understanding of the temperature regimes and the area distribution, as well as the order of magnitude of the various radiances from both rivers and power plants, can be observed which should lead to a better definition of temperature standards and site placement of power plants.

Associated with these temperature patterns are color patterns due to the different algal communities and sand suspensions. With a multispectral scanner we can map the distribution of water masses by their spectral signatures. This is illustrated in Fig. 18 where the different tones correspond to different water masses inshore and offshore. In some cases, eddy features are enhanced and the possibility of relating chlorophyll patterns to temperature patterns is now possible with multispectral sensors.

We have seen in the figures shown the potential for multispectral remote sensing to provide the type of information that is needed in understanding some very complicated problems in the marine environment. As NASA develops further capabilities with spaceborne multispectral sensors, we expect these examples to be important in other parts of the U.S. and to play their role in helping to manage our environment.

REFERENCES

1. Nalepka, R. F. 1970. "Investigation of Multispectral Discrimination Techniques." Infrared and Optics Laboratory, Willow Run Laboratories Institute of Science and Technology, The University of Michigan, Ann Arbor, Michigan, January 1970.

2. Burge, W. G. and W. L. Brown. 1970. "A Study of Waterfowl Habitat in North Dakota Using Remote Sensing Techniques." Final Report 1 May 1969 - 31 January 1970. Report # 2771-7-F, Infrared and Optics Laboratory, Willow Run Laboratories, Institute of Science and Technology, The University of Michigan, Ann Arbor, Michigan, July 1970.

3. Horvath, R., W. L. Morgan, and S. R. Stewart. 1971. "Optical Remote Sensing of Oil Slicks: Signature Analysis and Systems Evaluation." Final Report on Project 724104.2/1. Prepared for: U. S. Coast Guard Headquarters, prepared by: Willow Run Laboratories, Institute of Science and Technology, The University of Michigan, Ann Arbor, Michigan. October 1971.

4. Higer, A. L., M. C. Kolipinski, N. S. Thomson, and L. Purkerson. 1971. "Use of Processed Multispectral Scanner Data With a Digital Simulation Model for Forecasting Thermally Induced Changes In Benthic Vegetation in Biscayne Bay, Florida." In the Proceedings of the Seventh International Symposium on Remote Sensing of Environment, Ann Arbor, Michigan. p. 2055, May 1971.

5. Brown, W. L., F. C. Polcyn, A. N. Sellman, and S. R. Stewart. 1971. "Water Depth Measurement by Wave Refraction and Multispectral Techniques." Infrared and Optics Laboratory, Willow Run Laboratories, Institute of Science and Technology, University of Michigan, Ann Arbor, Michigan. Prepared for: NASA Manned Spacecraft Center, Technical Report 03165-31-T, August 1971.

a) .32 – .38 µm

b) .45 – .47 µm

c) .55 – .58 µm

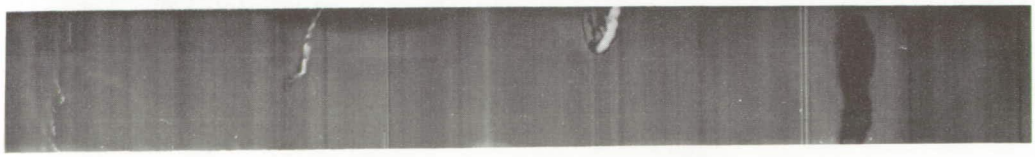

d) 9.3 – 11.7 µm

MULTISPECTRAL IMAGERY OF FOUR OILS

ALTITUDE: 2000 ft. DATE: 10/28/70 TIME: 1212

FROM L. to R.: 9.7 gravity fuel oil, 21.6 gravity crude oil, 26.1 gravity crude oil, diesel fuel

FIGURE 1

FIGURE 2

UNDERWATER VEGETATION MAPPING IN BISCAYNE BAY USING ANALOG COMPUTER PROCESSING OF MULTI-SPECTRAL DATA (Black represents coastlines; original map was in color.)

0.40 to 0.44 μ

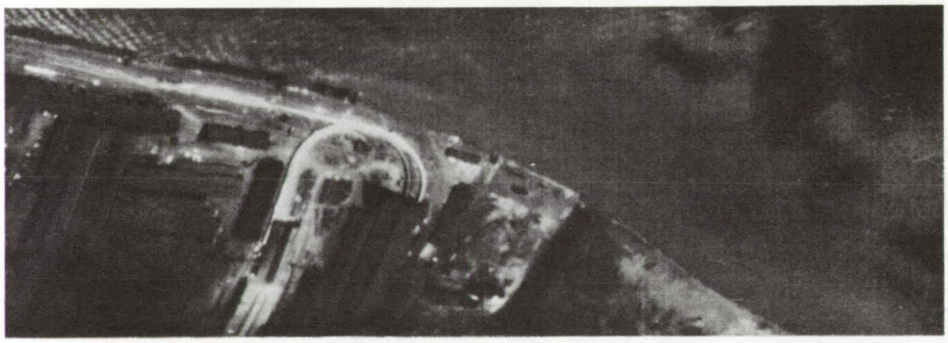

0.55 to 0.58 μ

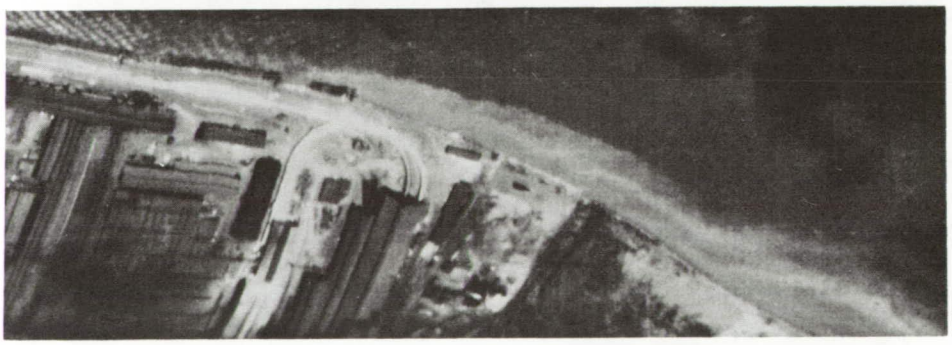

0.62 to 0.66 μ

Multispectral Comparison of Effluent Contrast

Infrared and Optics Laboratory

Willow Run Laboratories

THE INSTITUTE OF SCIENCE AND TECHNOLOGY
THE UNIVERSITY OF MICHIGAN

FIGURE 3

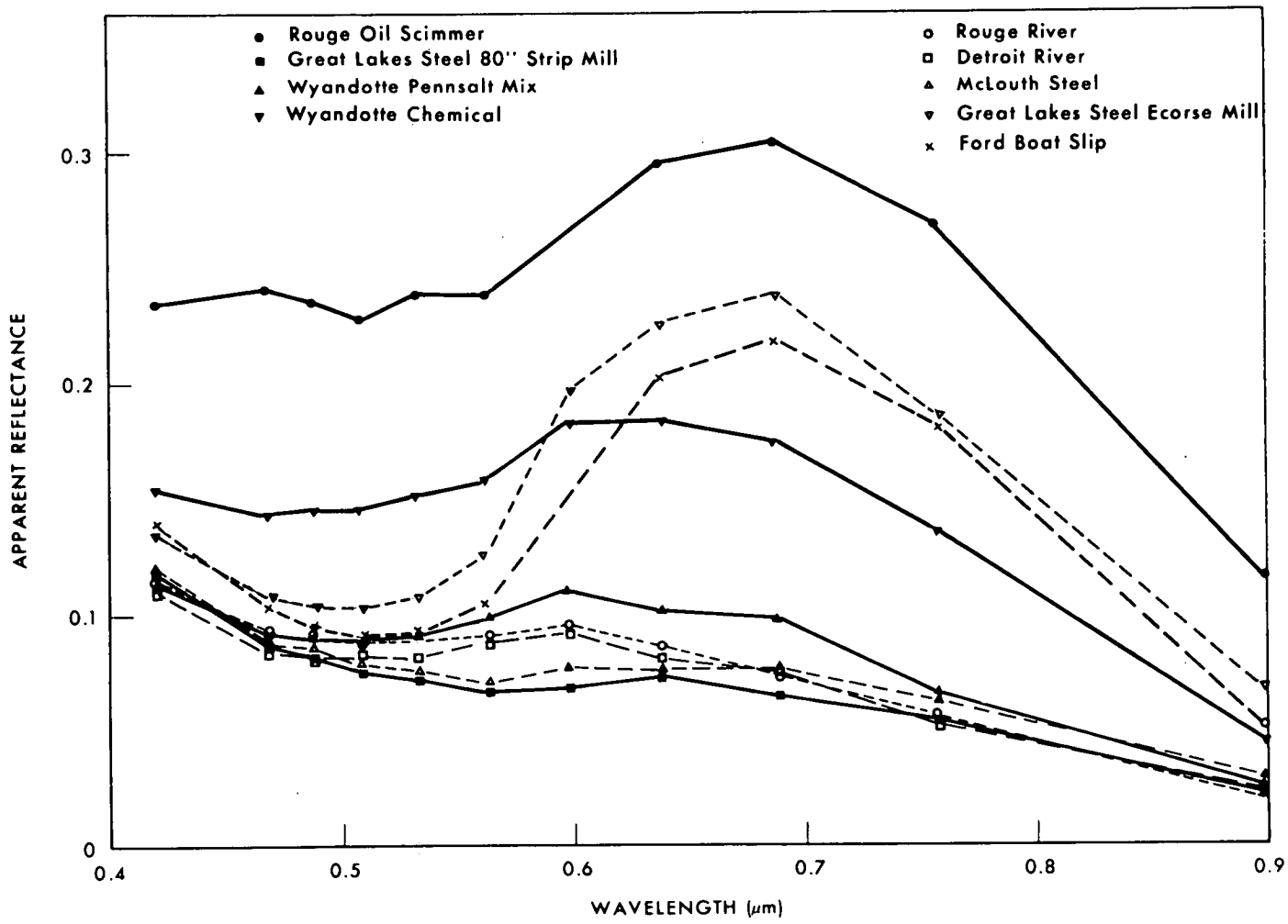

COMPARISON OF SPECTRA OF MAJOR POLLUTANTS IN ROUGE AND DETROIT RIVERS

Infrared and Optics Laboratory — Willow Run Laboratories — THE INSTITUTE OF SCIENCE AND TECHNOLOGY, THE UNIVERSITY OF MICHIGAN

FIGURE 4

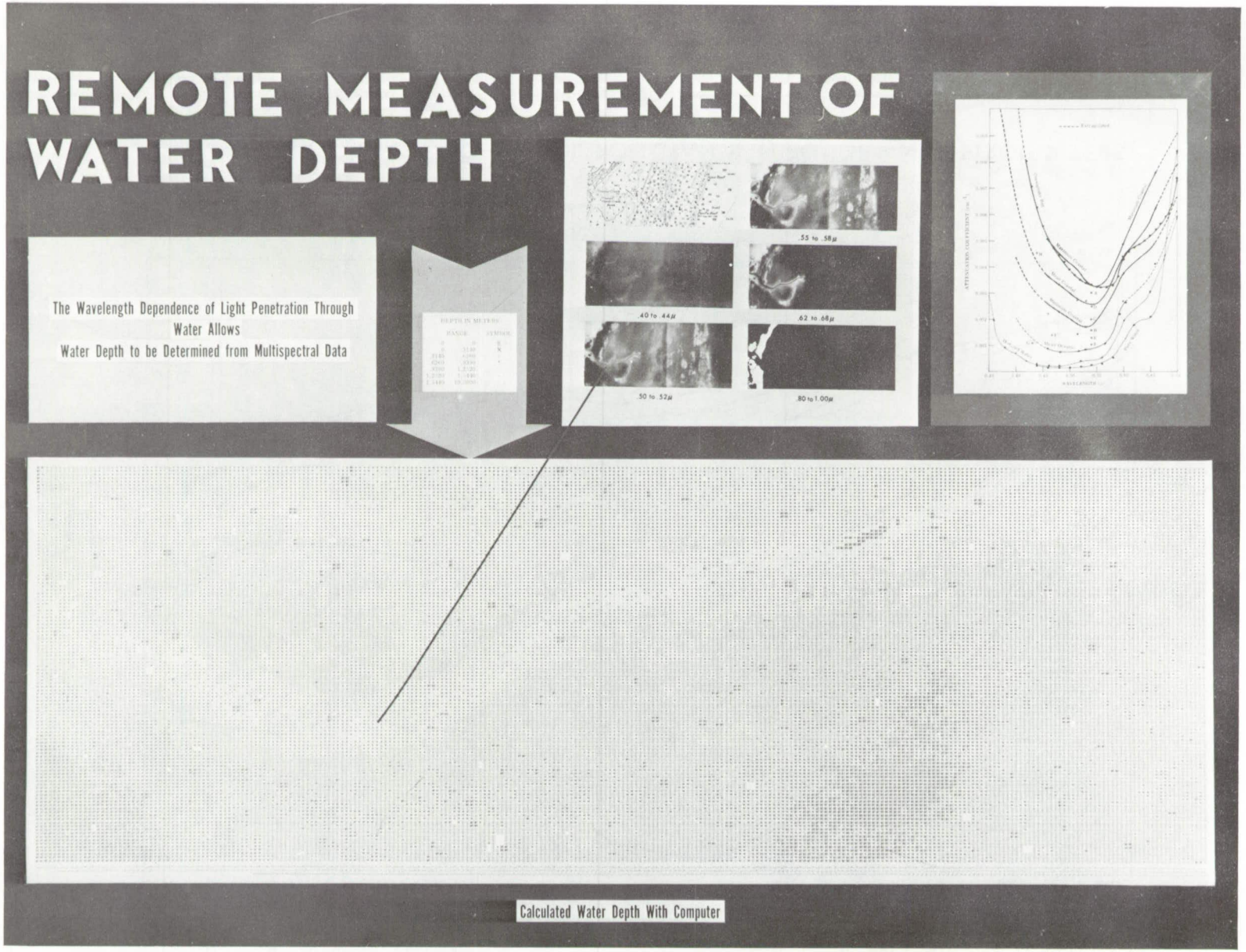
REMOTE MEASUREMENT OF WATER DEPTH
The Wavelength Dependence of Light Penetration Through Water Allows
Water Depth to be Determined from Multispectral Data
.55 to .58μ
.40 to .44μ
.62 to .68μ
.50 to .52μ
.80 to 1.00μ
Calculated Water Depth With Computer

FIGURE 5

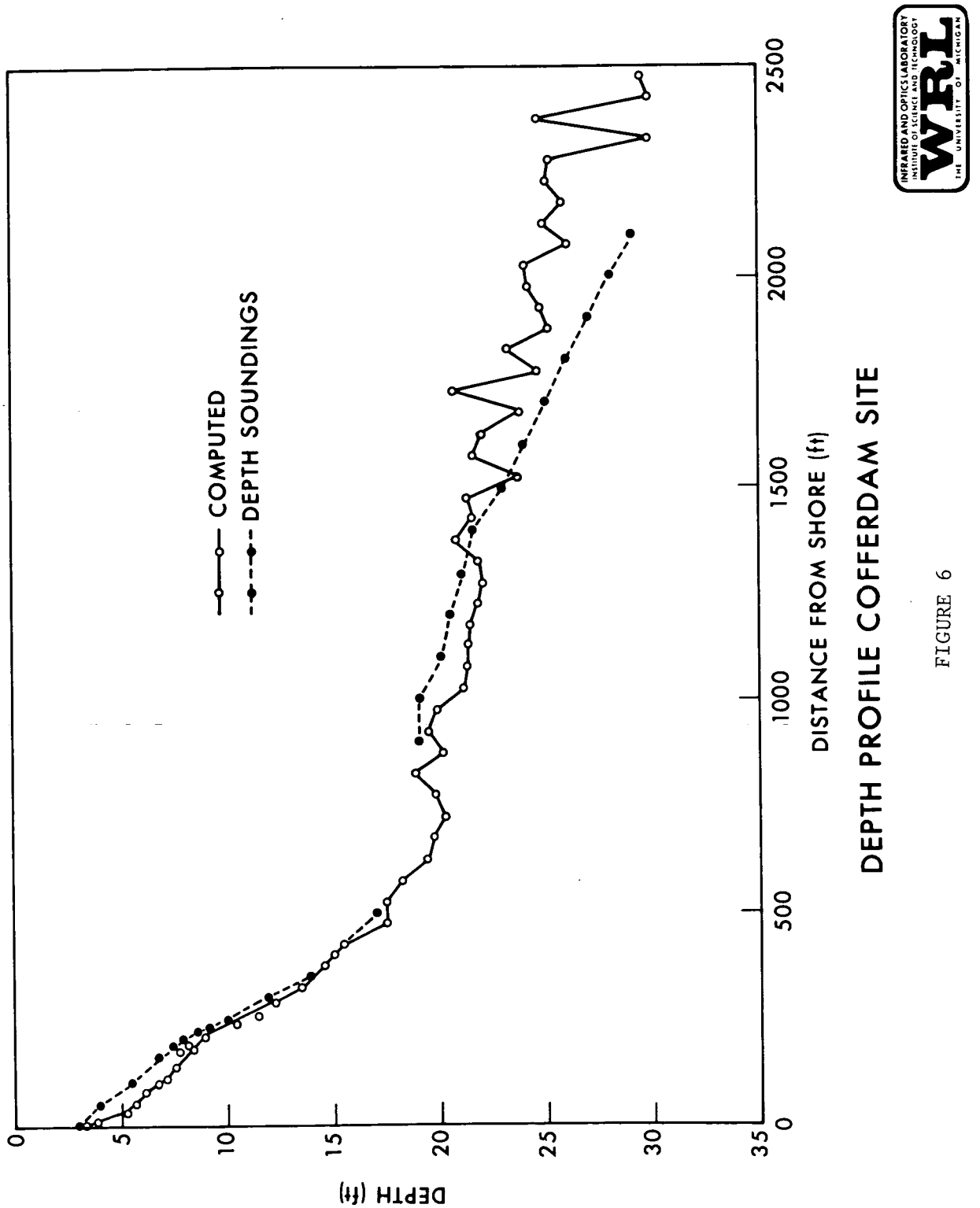
COMPUTED
DEPTH SOUNDINGS
DEPTH (ft)
0
5
10
15
20
25
30
35
0
500
1000
1500
2000
2500
DISTANCE FROM SHORE (ft)
DEPTH PROFILE COFFERDAM SITE

FIGURE 6

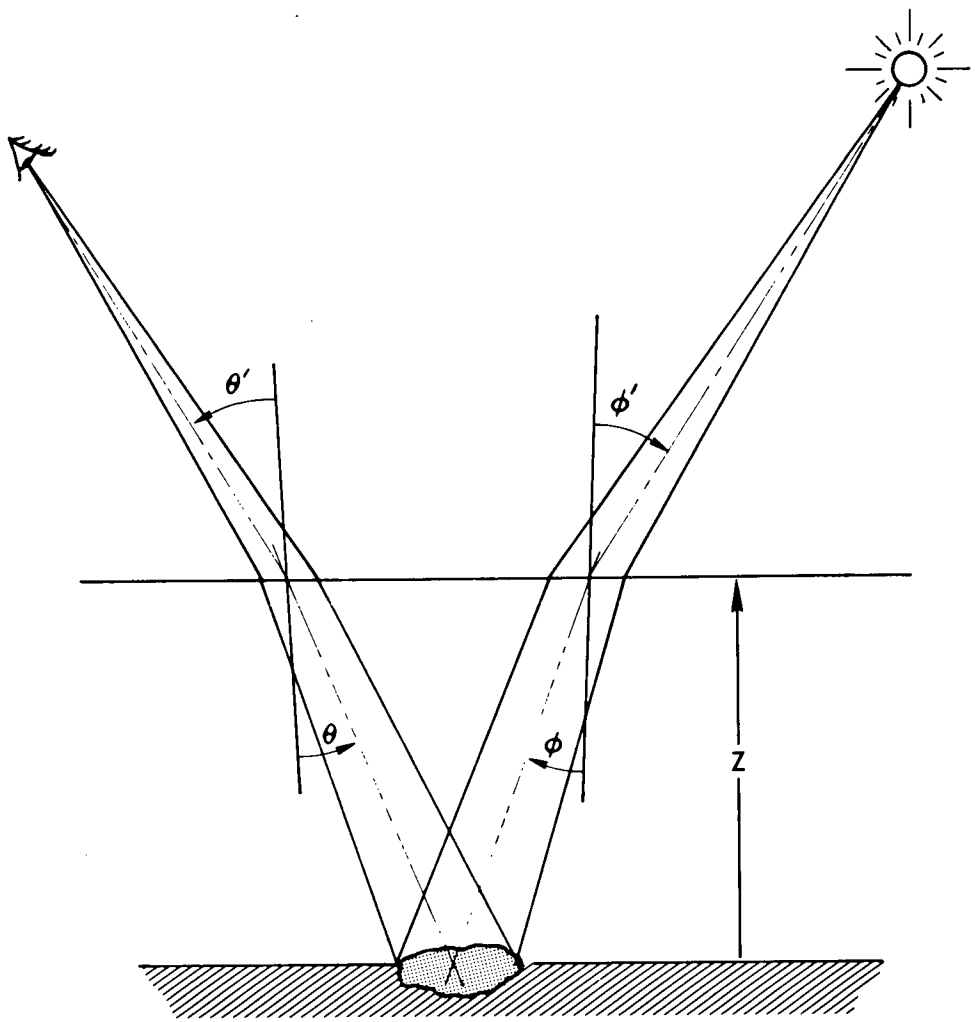

SCHEMATIC REPRESENTATION OF THE OBERVATION OF REFLECTED SUNLIGHT BY A REMOTE SENSOR

FIGURE 7

INFRARED AND OPTICS LABORATORY
INSTITUTE OF SCIENCE AND TECHNOLOGY
WRL
THE UNIVERSITY OF MICHIGAN

$$V_i(z) = \left(\frac{V_{ss}}{\rho_{ss}}\right)_i \rho_i e^{-\alpha f(\theta,\phi) z}$$

where

$$\rho_i = \rho_b - \frac{s}{\alpha} \frac{1}{4\pi \cos\phi f(\theta, \phi)}$$

FIGURE 8

CALCULATION OF REFLECTANCE ρ_i IN PRESENCE OF SCATTERING, s, AND BOTTOM REFLECTION ρ_B

z = depth of water

V_{ss}, ρ_{ss} are sun sensor voltage response and reflectance

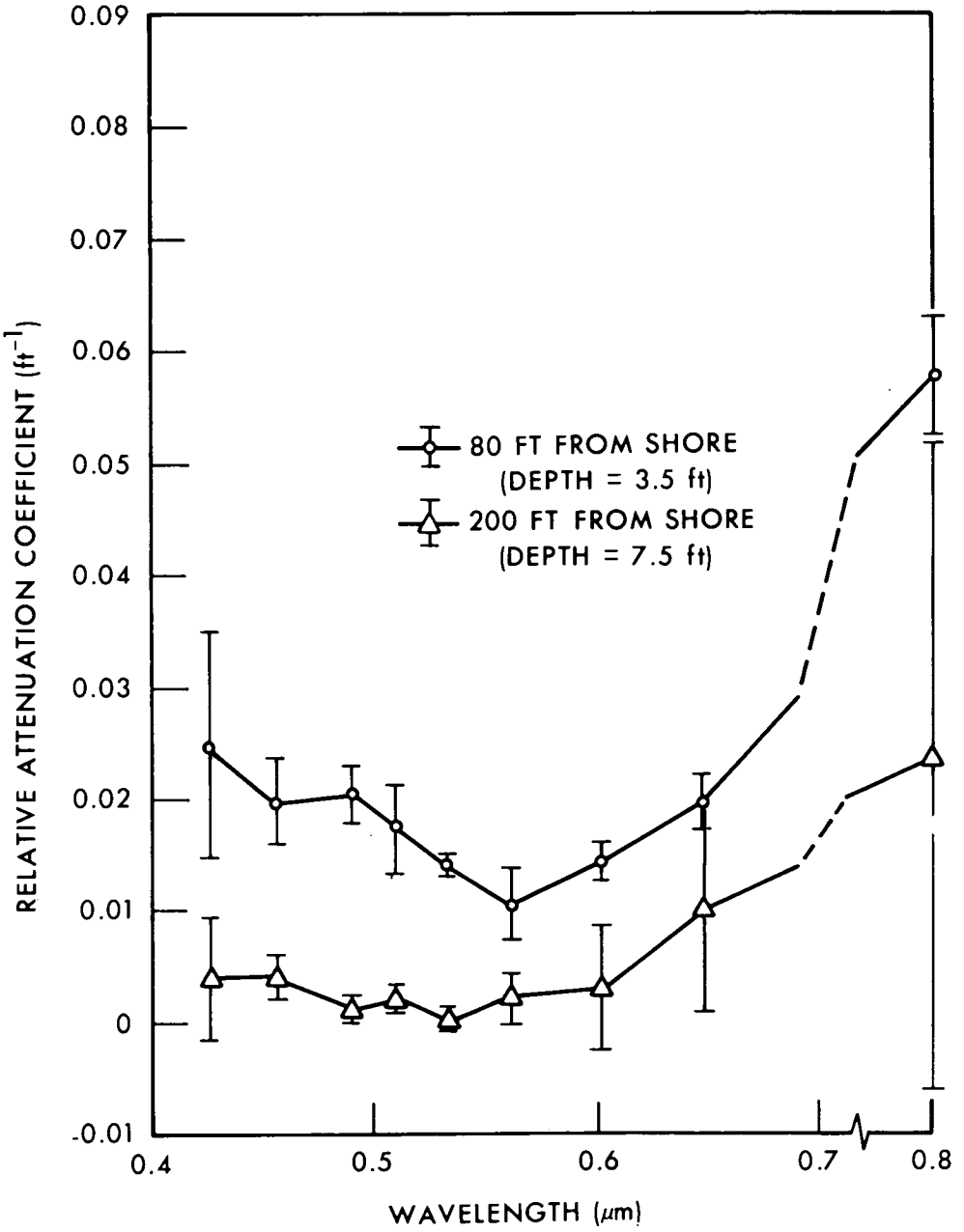

ATTENUATION COEFFICIENTS (COMPUTED) COFFERDAM SITE

FIGURE 9

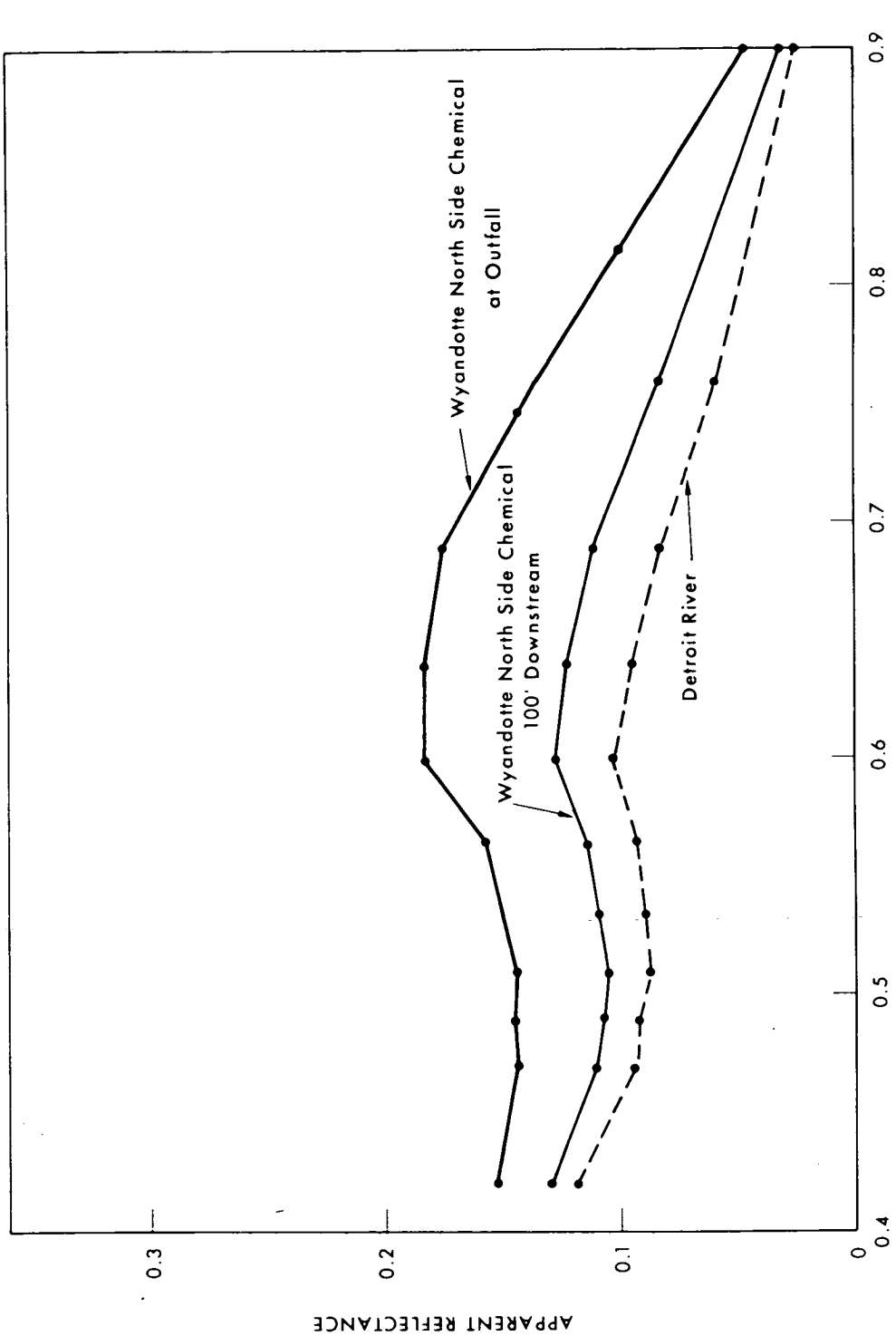

SPECTRA OF WYANDOTTE NORTH SIDE CHEMICAL SHOWING CONCENTRATION DIFFERENCES

Infrared and Optics Laboratory — *Willow Run Laboratories* — THE INSTITUTE OF SCIENCE AND TECHNOLOGY / THE UNIVERSITY OF MICHIGAN

FIGURE 10

FIGURE 11

HIGH ALTITUDE PHOTOGRAPH OF
MICHIGAN COASTLINE NEAR FRANKFORT,
MICHIGAN (Mission 103)

FIGURE 12

HIGH ALTITUDE PHOTOGRAPH OF
OUTFALLS OF THE MUSKEGON AND GRAND
RIVERS INTO LAKE MICHIGAN

FIGURE 13

EVIDENCE OF BEACH EROSION BY SHORE CURRENTS NEAR BIG SABLE PT.

FIGURE 14

SUN GLITTER DISCONTINUITY GIVING
EVIDENCE OF SHORE CURRENT

FIGURE 15

ENTRAPMENT OF RIVER OUTFALL BY
NEARSHORE CURRENT PREVENTS MIXING
WITH DEEPER LAKE WATERS

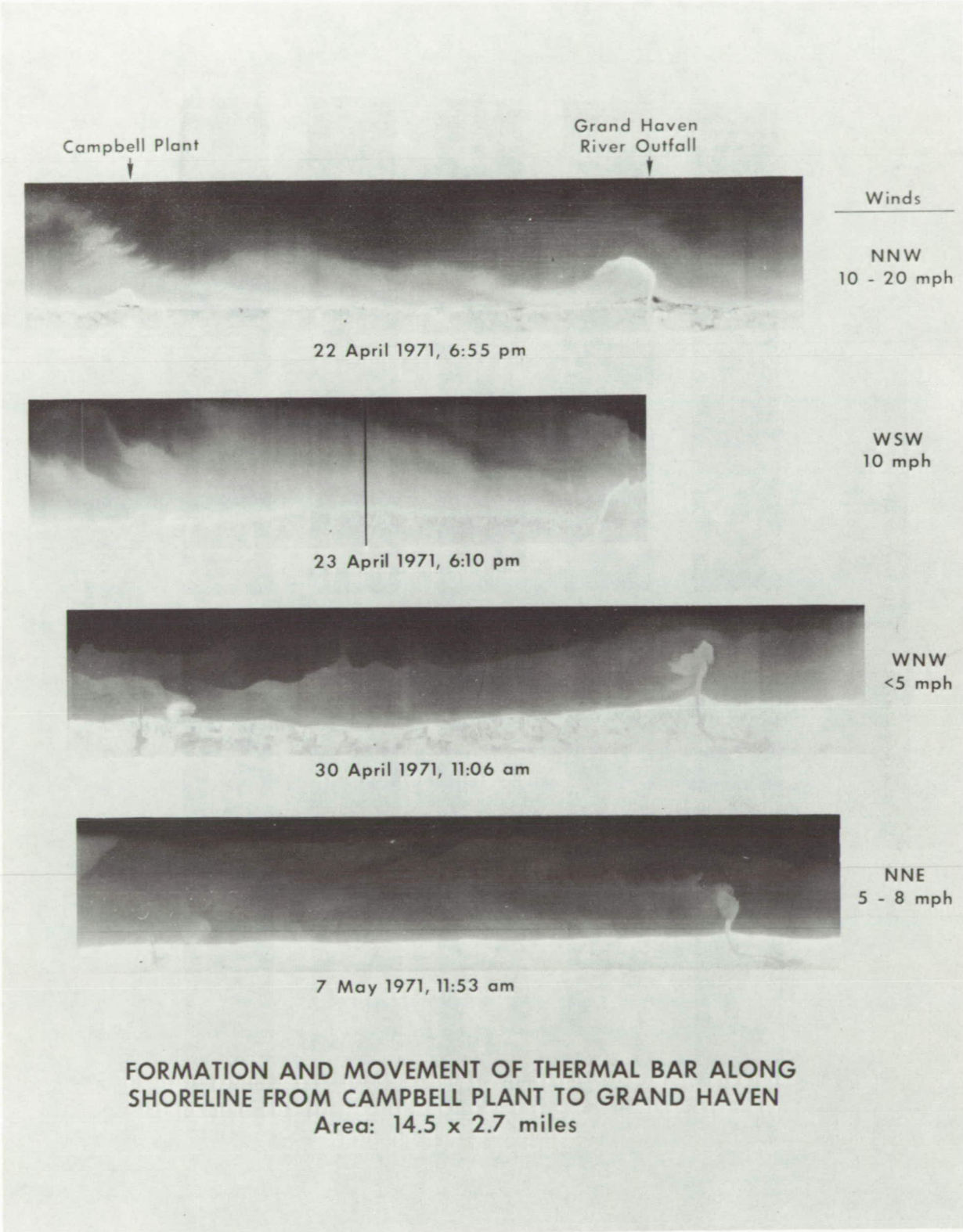
Campbell Plant
Grand Haven
River Outfall
Winds
NNW
10 - 20 mph
22 April 1971, 6:55 pm
WSW
10 mph
23 April 1971, 6:10 pm
WNW
<5 mph
30 April 1971, 11:06 am
NNE
5 - 8 mph
7 May 1971, 11:53 am
FORMATION AND MOVEMENT OF THERMAL BAR ALONG
SHORELINE FROM CAMPBELL PLANT TO GRAND HAVEN
Area: 14.5 x 2.7 miles

FIGURE 16

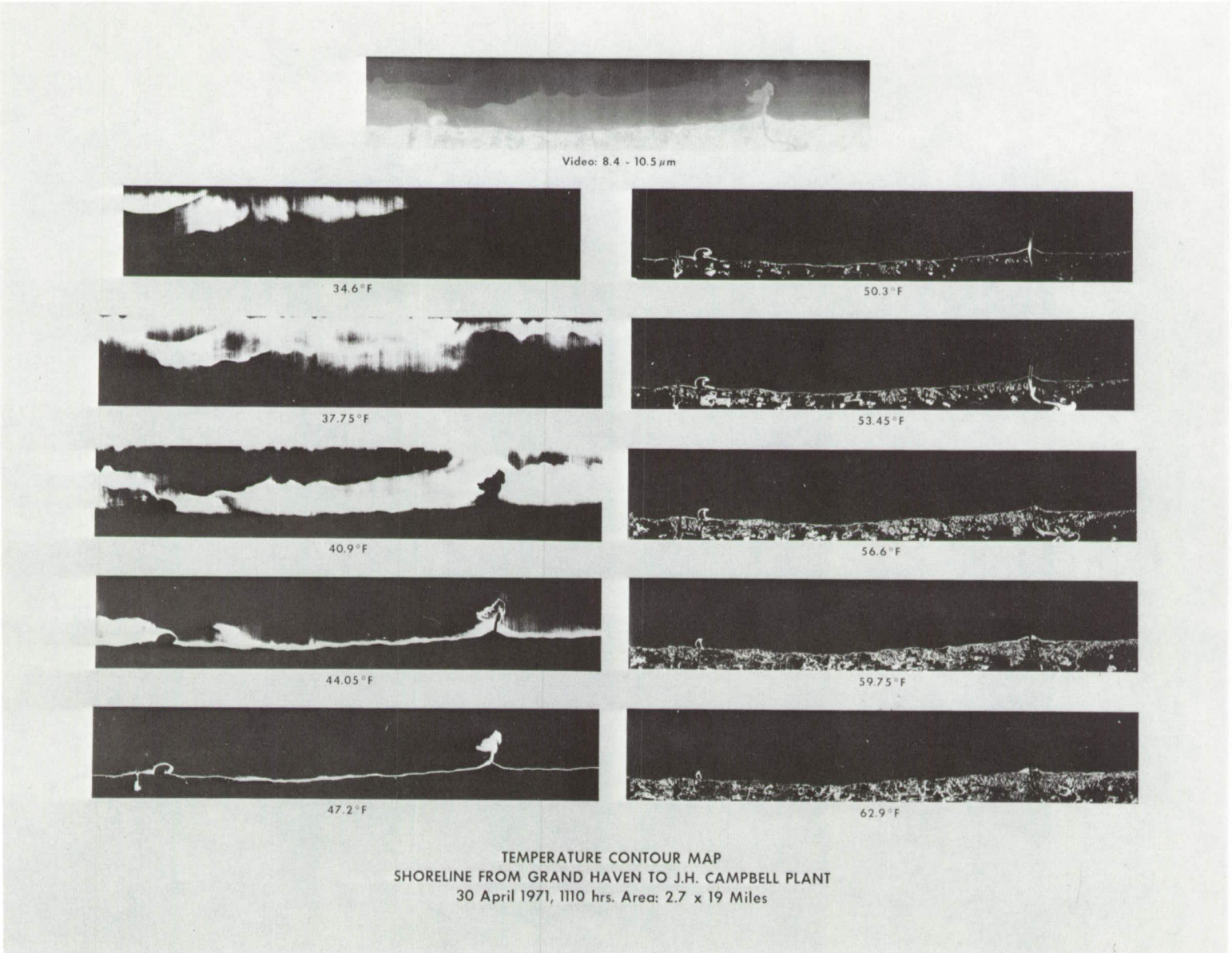

TEMPERATURE CONTOUR MAP
SHORELINE FROM GRAND HAVEN TO J.H. CAMPBELL PLANT
30 April 1971, 1110 hrs. Area: 2.7 x 19 Miles

FIGURE 17

FIGURE 18

ZONES OF WATER MASSES ALONG
MICHIGAN SHORELINE ENHANCED BY
MULTISPECTRAL PROCESSING